analytical chemistry

ARTICLE

pubs.acs.org/ac

Impact of DNA−Surface Interactions on the Stability of DNA Hybrids

Sarah M. Schreiner,[†] Anna L. Hatch,[†] David F. Shudy,[†] David R. Howard,[‡] Caitlin Howell,[§,∥] Jianli Zhao,[∥] Patrick Koelsch,[§,∥] Michael Zharnikov,[∥] Dmitri Y. Petrovykh,[*,⊥,▽] and Aric Opdahl[*,†]

[†]Department of Chemistry and [‡]Department of Biology, University of Wisconsin—La Crosse, La Crosse, Wisconsin 54601, United States

[§]Institute of Toxicology and Genetics, Karlsruhe Institute of Technology, Hermann-von-Helmholtz-Platz 1, 76344 Eggenstein-Leopoldshafen, Germany

[∥]Angewandte Physikalische Chemie, Universität Heidelberg, Im Neuenheimer Feld 253, 69120 Heidelberg, Germany

[⊥]Department of Physics, University of Maryland, College Park, Maryland 20742, United States

Supporting Information

ABSTRACT: The structure and stability of single- and double-stranded DNA hybrids immobilized on gold are strongly affected by nucleotide−surface interactions. To systematically analyze the effects of these interactions, a set of model DNA hybrids was prepared in conformations that ranged from end-tethered double-stranded to directly adsorbed single-stranded (hairpins) and characterized by surface plasmon resonance (SPR) imaging, X-ray photoelectron spectroscopy (XPS), fluorescence microscopy, and near edge X-ray absorption fine structure (NEXAFS) spectroscopy. The stabilities of these hybrids were evaluated by exposure to a series of stringency rinses in solutions of successively lower ionic strength and by competitive hybridization experiments. In all cases, directly adsorbed DNA hybrids are found to be significantly less stable than either free or end-tethered hybrids. The surface-induced weakening and the associated asymmetry in hybridization responses of the two strands forming hairpin stems are most pronounced for single-stranded hairpins containing blocks of *m* adenine (A) nucleotides and *n* thymine (T) nucleotides, which have high and low affinity for gold surfaces, respectively. The results allow a qualitative scale of relative stabilities to be developed for DNA hybrids on surfaces. Additionally, the results suggest a route for selectively weakening portions of immobilized DNA hybrids and for introducing asymmetric hybridization responses by using sequence design to control nucleotide−surface interactions—a strategy that may be used in advanced biosensors and in switches or other active elements in DNA-based nanotechnology.

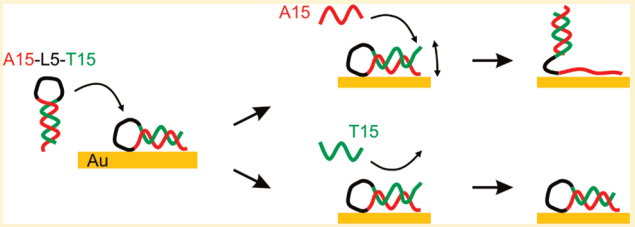

The ability to predict the stability of a DNA hybrid in solution underpins its emerging use as a structural, addressable, or active material rather than as a biological carrier of genetic information.[1−4] Structured DNA hybrids immobilized on surfaces offer a promise of practical miniaturized devices that employ DNA in specific hybridized or folded states, e.g., molecular beacons, aptamers, molecular walkers and motors, or self-assembled nanostructures.[3−6]

Immobilization and hybridization of DNA on surfaces have been studied extensively;[7−14] however, the influence of DNA−surface interactions on the *stability* of DNA hybrids has been observed but not systematically analyzed.[6,15−19] A significant challenge for comparing DNA hybrids on surfaces and in solutions is designing methods to systematically vary DNA−surface interactions so that their effects on stability can be isolated. Replication of solution-based stability measurements for DNA hybrids on surfaces is hindered by the additional challenges of adapting surface-based analytical methods to experiments involving *continuous* changes in solution parameters, such as temperature or ionic strength, which are typically used to destabilize and denature DNA hybrids in solution experiments.

We have previously developed a practical approach for controlling and analyzing the structure and stability of DNA hybrids immobilized on gold.[15] Our model DNA strands typically include homonucleotide sequences (blocks), which simplify spectroscopic characterization[8,11,20−22] and allow the differential affinities of homo-oligonucleotides for gold to be exploited.[11,15,20]

Here, we demonstrate that DNA−surface interactions can dramatically destabilize DNA hybrids immobilized on gold. We are able to quantitatively compare the stability of DNA hybrids as a function of their immobilized conformations by using a model set of DNA probes and hybrids that were designed to adopt different conformations on gold, while sharing the same A15:T15 composition. The nucleotide-dependent interactions of these sequences with gold are used to prepare surface hybrids in a wide range of conformations (Figure 1). We infer the stabilities of these conformations by analyzing their hybridization behavior in situ by surface plasmon resonance (SPR) imaging[15] and support

Received: April 22, 2011
Accepted: April 26, 2011
Published: May 11, 2011

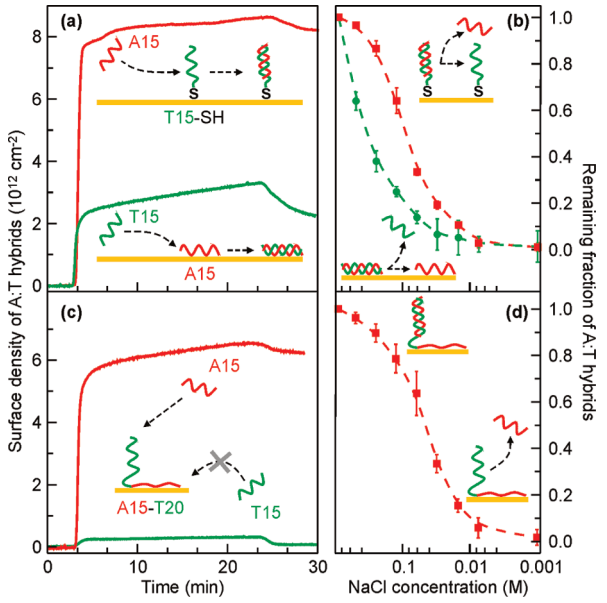

Figure 1. Formation and stability of A:T hybrids immobilized on gold in different surface conformations. Diagrams depict idealized representations of each target−probe pair (red = adenine, green = thymine) before and after hybridization (a, c) and during denaturing (b, d). The line and symbol colors correspond to the color-coding of the respective targets: A15 (red) or T15 (green). In each hybridization experiment (a, c), the sensor was exposed for ca. 20 min to 4 μM solution of a target in 1 M NaCl-TE, followed by a rinse for ca. 5 min in blank buffer (note the removal of weakly bound DNA targets after ca. 25 min). Stringency rinse data (b, d) were obtained by exposing *prehybridized* SPR sensors to solutions of successively lower ionic strength (NaCl concentration) and monitoring the fraction of the original A:T hybrids remaining on the surface upon returning to the blank 1 M NaCl-TE buffer. Error bars in b and d represent variation among replicate samples.

these inferences by ex situ spectroscopic analysis[8,20−22] and by complementary measurements for hybrids based on a mixed sequence of 15 nucleotides. We expect the trends in formation and stability of DNA hybrids on surfaces observed here to be relevant for designing DNA-based biosensors, materials, and nanotechnology,[1−6,17] all of which utilize competitive, invasive, or asymmetric hybridization, i.e., the solution counterparts of the processes that we investigate for surface hybrids.

EXPERIMENTAL DETAILS

Materials. Commercial purified oligonucleotides included the following sequences: 15-nucleotide homo-oligonucleotides of adenine (A15) and thymine (T15); a mixed sequence of 15 nucleotides (5′-CAATGCAGATACACT-3′, denoted P15) and full complement for P15 (5′-AGTGTATCTGCATTG-3′, denoted P15′). These sequences were incorporated as hybridization "blocks" into longer strands, including A15−T20, P15′−A5−P15, and P15−T5−P15′ (all sequences written in the 5′ to 3′ direction). Buffers denoted NaCl-TE and $CaCl_2$-TE contained 1 M NaCl or $CaCl_2$, respectively, 1× TE (10 mM Tris·HCl, 1 mM EDTA), and were adjusted to pH 7 with HCl. Additional materials and modified oligonucleotides are described in the Supporting Information.

Sample Preparation. Gold substrates were cleaned as described previously (see the Supporting Information).[8,11,15] Unmodified oligonucleotides were immobilized on clean gold surfaces for 20 h at 35 °C (4 μM DNA in $CaCl_2$-TE).[11,15] To remove calcium ions and weakly bound DNA, each sample was rinsed sequentially with deionized water, NaCl-TE, 0.1 M NaOH, and deionized water, before drying under flowing nitrogen. Thiol-modified oligonucleotides were immobilized for ca. 2 h at room temperature (4 μM DNA in NaCl-TE). Preparation of samples for NEXAFS and fluorescence measurements is described in the Supporting Information.

Measurements. DNA immobilization and hybridization were measured in situ using an SPR imaging system (GWC, Madison, WI) as described previously.[15] Our quantitative analysis[15] followed established methods outlined by Jung et al.[23] Instrumentation and procedures for laser-scanning confocal fluorescence microscopy, X-ray photoelectron spectroscopy (XPS), and near edge X-ray absorption fine structure (NEXAFS) spectroscopy are described in the Supporting Information.[11,21,24,25]

RESULTS

Our investigation of how the stability and structures of DNA hybrids are affected by their interactions with gold surfaces included four major components: design and preparation of model hybrids, *direct* measurements of their stabilities, competitive measurements of their *relative* stabilities, and complementary in situ and ex situ measurements of DNA structure and conformation.

Double-Stranded Hybrids: Conformations. The dramatic difference between the affinities of adenine and thymine homo-oligonucleotides for gold,[10,11,20,26,27] makes A15 and T15 sequences particularly suitable for preparing model double-stranded hybrids in two conformations (Figure 1a).

Unmodified A15 oligonucleotides have high affinity for gold and adopt directly adsorbed (flat) conformations.[11,20,28] The surface density of A15 probes measured by SPR (immobilization data not shown) is 1.3×10^{13} cm^{-2}, in agreement with previously reported (dA) nucleotide surface densities on gold.[11,20,29] Hybridization of T15 targets with directly adsorbed A15 probes (green line in Figure 1a) results in a hybrid density of 1.8×10^{12} cm^{-2} (observed after the posthybridization buffer rinse); the low yield of ca. 15% is consistent with hybridization being suppressed by DNA−surface interactions.[7,15,30] The expected directly adsorbed conformation of the resulting *double-stranded* A15:T15 hybrids is schematically indicated in Figure 1a (bottom). In agreement with previous observations,[15] noncomplementary P15′ targets produced no detectable hybrids with A15 probes (Figure S1, Supporting Information).

The low affinity for gold of thymine homo-oligonucleotides[20] results in predominantly end-tethered conformations of thiolated T*n*−SH probes, when they are immobilized at sufficiently high surface densities.[8,10,22,27] For a close comparison to the directly adsorbed A15:T15 hybrids in Figure 1a, the T15−SH probes were immobilized at a density of 1.4×10^{13} cm^{-2} (immobilization SPR data not shown), which produced 8.0×10^{12} cm^{-2} density of A15:T15−SH hybrids (red line in Figure 1a). The hybridization yield is much higher for T15−SH than for A15 (56% vs 15%, respectively), in agreement with the expected higher accessibility of end-tethered probes.[7,8,15,22]

Double-Stranded Hybrids: Stability. The stability of DNA hybrids can be evaluated by using a series of stringency rinses in solutions of successively lower ionic strength.[15] Figure 1b illustrates the application of this method for evaluating the stability of model A:T hybrids in directly adsorbed and end-tethered

conformations. Tracking the reduced density of hybrids after each stringency rinse provides an analog of a melting curve, except one produced by destabilizing DNA hybrids *electrostatically* rather than thermally.[15]

The shift between the denaturing curves in Figure 1b clearly indicates that A:T hybrids are less stable in directly adsorbed than in end-tethered conformation. For a quantitative comparison, we use the ionic strength at which 50% of the hybrids become denatured, i.e., a parameter equivalent to the melting temperature in thermal denaturing. We observe that 50% of the directly adsorbed A15:T15 hybrids are denatured in ca. 0.5 M NaCl (green curve in Figure 1b), which is similar to ionic strength of some *hybridization* buffers. In contrast, the end-tethered A15:T15−SH hybrids require reducing the NaCl concentration below 100 mM to denature 50% of the hybrids (red curve in Figure 1b).

The generality of the stability trends observed in Figure 1b is confirmed by the qualitatively similar results of control experiments with complementary P15 and P15′ sequences that have mixed nucleotide compositions (Figure S2, Supporting Information). The destabilization of the directly adsorbed double-stranded hybrids in Figure 1b is thus not produced exclusively by the high affinity of (dA) blocks for gold or by the repetitive sequences of the A15:T15 hybrids.

Competitive Measurements of Relative Stabilities. The *direct* stability measurements illustrated in Figure 1b are not readily applicable to all types of DNA hybrids. Accordingly, we adapt competitive hybridization for assessing *relative stabilities* of DNA hybrids on surfaces, as illustrated by comparing the responses of surfaces functionalized with T15−SH (Figure 2a) and A15 (Figure 2b) probes to a series of three hybridization challenges by two targets (T15, then A15, then T15). To minimize differences in electrostatic effects, identical solution conditions and comparable probe densities are used for experiments in Figure 2.

For T15−SH probes, the initial introduction of noncomplementary T15 targets (vertical green arrow at ca. 5 min in Figure 2a) does not produce a detectable SPR signal. Complementary A15 targets (introduced at ca. 30 min in Figure 2a) produce A15:T15−SH hybrids at a surface density similar to that in Figure 1a. These *end-tethered* double-stranded hybrids are then challenged by T15 targets (at ca. 60 min in Figure 2a), but the slow decrease of the SPR signal indicates that the end-tethered A15:T15−SH hybrids are minimally affected by this competitive hybridization challenge, which provides a potential pathway for A15 to leave the end-tethered surface hybrids and form *solution hybrids* instead.

The directly adsorbed A15 probes in Figure 2b respond to the initial introduction of complementary T15 targets, producing T15:A15 hybrids at a surface density similar to that in Figure 1a (note the expanded vertical scale in Figure 2b). These directly adsorbed hybrids are then challenged by A15 targets (introduced at ca. 30 min in Figure 2b), which provide a pathway for the T15 part of the directly adsorbed hybrid to leave the surface by forming solution hybrids. In contrast to the minimal response to a similar challenge in Figure 2a, the directly adsorbed T15:A15 hybrids are readily and *completely* disrupted by the competitive solutions targets, as indicated by the signal returning to the baseline at ca. 50 min. The original directly adsorbed A15 probes "recycled" by this competitive step are then available for hybridization with T15 targets (introduced at ca. 55 min), producing the same surface density of hybrids in both hybridization cycles.

The generality of the trends in Figure 2 is confirmed in control experiments with P15:P15′ hybrids of mixed nucleotide compositions

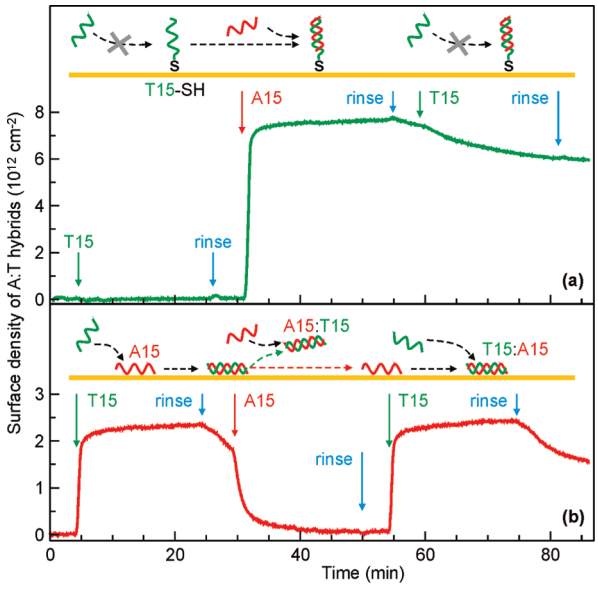

Figure 2. Competitive hybridization challenges applied to double-stranded A:T hybrids in end-tethered and directly adsorbed conformations. Diagrams depict idealized representations of each target−probe pair (red = adenine, green = thymine) through a series of three hybridization challenges. Data plots are color-coded by probes: green for T15−SH in a and red for A15 in b; note the expanded vertical scale in b. In each experiment, the SPR sensor was sequentially exposed to T15 target (vertical green arrows at ca. 5 min); blank 1 M NaCl-TE (cyan arrows at ca. 25 min); A15 target (red arrows at ca. 30 min); blank 1 M NaCl-TE (cyan arrows at ca. 50−55 min); T15 target (green arrows at ca. 55−60 min); and the final rinse in blank 1 M NaCl-TE (cyan arrows after ca. 75−80 min). Hybridization conditions were the same as those in Figure 1a. Immobilization of the probes not shown; baseline SPR signals are from freshly prepared probe surfaces after a rinse in blank buffer.

(Figure S3, Supporting Information). When challenged with a solution of P15 targets, the end-tethered P15′:P15−T5−SH hybrids are barely affected, while the directly adsorbed P15′:P15 hybrids are nearly completely disrupted.

Single-Stranded A:T Hybrids. The dramatic destabilization of directly adsorbed double-stranded hybrids in Figures 1a and b and 2 suggests that surface interactions should similarly destabilize *single-stranded* DNA hybrids. To determine how single-stranded hybrids are affected by nucleotide−surface interactions, we designed and characterized a series of sequences based on the A*m*−T*n* motif.

In solution, the self-complementary regions of A*m*−T*n* sequences fold into a hairpin conformation, forming an intramolecular single-stranded hybrid.[11] Previous ex situ FTIR and XPS measurements of A*m*−T*n* strands revealed that their adsorption on gold primarily involves the adenine nucleotides.[11] Attachment to gold via (dA) blocks has also been demonstrated for similarly constructed strands with T*n* section replaced by mixed-composition P15 probe sequences (Figure S4, Supporting Information).[15] The hybridization behavior and conformations of self-complementary A*m*−T*n* sequences immobilized on gold can be expected to fall within the range between the limiting cases established in Figures 1a and b and 2.[15] Surface interactions may also change the typical *symmetric* and *low-yielding* hybridization response of folded hairpins in solution.

Interrogating Single-Stranded A:T Hybrids. We used an unmodified A15−T20 sequence to prepare model directly adsorbed

A:T hairpins for SPR measurements directly comparable to those summarized in Figures 1a and b and 2. In situ monitoring by SPR (in agreement with complementary ex situ XPS analysis in Figure S5, Supporting Information) indicates that A15−T20 strands immobilize at a saturation surface density of 1.3×10^{13} cm^{-2}, i.e., with a footprint identical to that of unmodified A15 probes in Figure 1a (and that of A15−T5−P15 probes in Figure S4, Supporting Information).[15] The similar footprints of sequences that include an A15 block are consistent with their immobilization on gold via the A15 block (diagram in Figure 1c).[11,15,20] Hybridization attempts with both A15 and T15 targets in Figure 1c are *competitive hybridization* experiments, as either target may have to invade the self-hybridized structure of the directly adsorbed A15−T20 hairpin, which is shown as opened in the schematic only to clarify the sections targeted in hybridization attempts.

When T20 blocks of directly adsorbed A15−T20 probes are interrogated by A15 targets, SPR data show a rapid hybridization (red line in Figure 1c) with a relatively efficient 45% yield (cf. 56% yield for T15−SH probes in Figure 1a). The corresponding denaturing curve in Figure 1d indicates that A15−T20:A15 hybrids are as stable as the end-tethered A15:T15−SH hybrids (cf. red line in Figure 1b), requiring the NaCl concentration to be reduced to 100 mM for denaturing 50% of the hybrids.

In contrast to the facile hybridization with A15 targets, no hybrids are detected by SPR when A15−T20 probes are interrogated by T15 targets (green line in Figure 1c), which can potentially form hybrids with the A15 block. In control experiments with similarly constructed but not self-complementary A15−T5−P15 probes, weak T15:A15−T5−P15 hybrids are formed with T15 targets (Figure S4, Supporting Information).[15]

The highly asymmetric hybridization behavior of the (dA) and (dT) blocks of the A15−T20 sequence in Figure 1c suggests that directly adsorbed A*m*−T*n* sequences can undergo a transition from the self-hybridized "closed" hairpin state to a roughly L-shape conformation (attached to gold via A15 block), which is produced when the hairpin is destabilized, either by competitive hybridization (Figure 1c) or electrostatically (Figure 1d). Control experiments using fluorescence and NEXAFS provide additional evidence of such a transition (Figures S6−S8, Supporting Information).

Distance-dependent quenching for fluorescent molecules placed in proximity to a gold surface[13,31,32] allows us to track the proximity to the gold surface for the TAMRA-labeled 3′ terminal of a model A15−T30* sequence. In 1 M NaCl-TE buffer, no fluorescence is observed from the A15−T30* probes (Figure S6b, Supporting Information). The fluorescence signal from the A15−T30* probes can be reversibly enhanced by addition of A15 targets (Figure S6c, Supporting Information) or by replacing the NaCl-TE buffer with deionized water (Figure S6a, Supporting Information).

For a label-free evaluation of hybrids formed with A*m*−T*n* probes, we analyze NEXAFS features at the K-edge of nitrogen that are sensitive to the orientation and ordering of surface-immobilized DNA molecules (Figure S8, Supporting Information).[13,22,28,33] In particular, the difference between the spectra acquired at 20° and 90° angles of X-ray incidence conveniently visualizes the NEXAFS linear dichroism[34] for the characteristic π^* resonances of adenine and thymine.[22,28,33,35] A change from negative to positive dichroism is observed after A5−T15 probes are exposed to A15 targets (Figure S8b, Supporting Information), indicating that the initial in-plane orientation

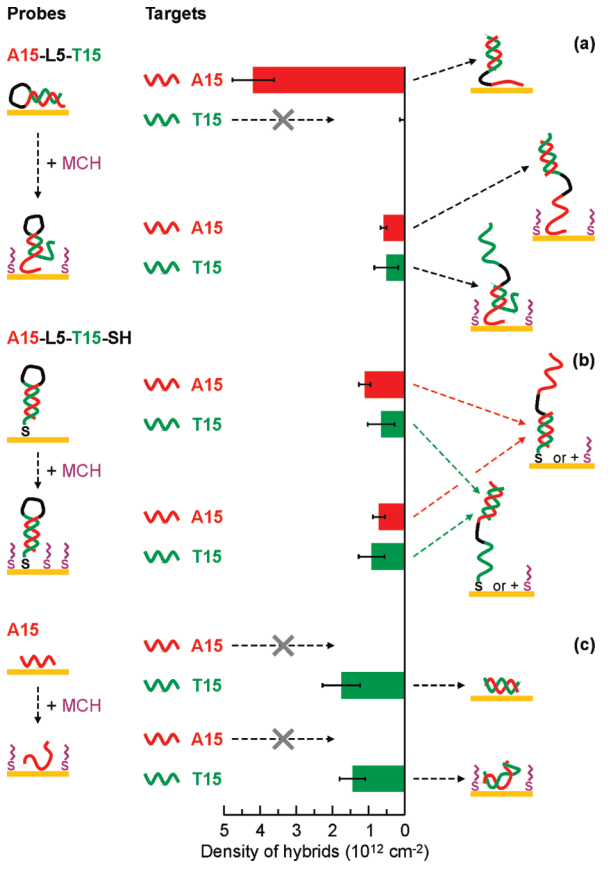

Figure 3. Testing hybridization responses of A15 and T15 sections of model probes immobilized in different conformations. SPR hybridization signals (bar plot) are compared for A15−L5−T15 (a), A15−L5−T15−SH (b), and A15 (c) probes in conformations adopted after deposition on bare gold (top set of data for each probe sequence) and after exposure to 1 mM MCH solution for 5 min (bottom set of data for each probe sequence). Diagrams depict idealized representations of each target−probe pair [red = adenine, green = thymine, black = L5 linkers (CATAC)] before (diagrams on the left) and after (diagrams on the right) hybridization, on bare gold and after MCH (purple in diagrams) treatment. Hybridization conditions were the same as those in Figure 1a. Bars are color-coded according to the respective targets (red = A15, green = T15); hybridization signals $<2 \times 10^{11}$ cm^{-2} are indicated by crossed-out horizontal arrows.

of the T15 block changes to one extended away from the surface upon hybridization with A15 (which also is extended away from the surface as part of the same hybrid). Furthemore, the negative dichroism observed for the A5 block of A5−T15 is consistent with the presumed in-plane orientation of the A5 attachment block, whereas after hybridization with the longer A15 targets, the (dA) component of the spectra is significantly increased and presumably dominated by the signal from the hybrids (Figure S8b, Supporting Information).

Controlling Surface Interactions for Single-Stranded A:T Hybrids. The experiments summarized in Figures 1 and 2 focused on comparing the behavior of hybrids that had the *same composition* (A15:T15) but different structures and conformations. In Figure 3 we use an alternative approach to discern the effects of surface interactions on properties of A:T hybrids, whereby the properties of the *same* self-complementary *sequence* are examined in conformations ranging from directly adsorbed to

end-tethered. The latter configuration is produced by backfilling the gold surface with a small thiolated molecule (1-mercapto-6-hexanol, MCH), which is a common method for reducing DNA−surface interactions.[7,9,12,13,31,32,36]

The two variants of single-stranded A15:T15 hybrids in Figure 3 are denoted A15−L5−T15 and A15−L5−T15−SH. Substituting the original T5 spacer of A15−T20 by a mixed L5 sequence (CATAC) eliminates the loop portion of the hairpin as a potential hybridization site for A15 targets. The thiolated variant provides an attachment mode other than via nucleotide−gold interactions; placement of the thiol at the T15 terminus helps to further reduce the ambiguity of the attachment mechanism.

The directly adsorbed A15−L5−T15 probes behave nearly identically to the A15−T20 probes in Figure 1c, displaying significant hybridization with A15 targets and no hybridization with T15 targets (Figure 3a). The hybridization behavior of the same sequence changes dramatically when it is immobilized on gold via a thiol, i.e., when A15−L5−T15 hairpins are end-tethered (Figure 3b). For A15−L5−T15−SH probes, hybridization attempts to both A15 and T15 blocks result in low and roughly symmetric yields, i.e., exhibiting behavior of folded hairpins with A:T stems, which are stable against invasion by A15 or T15 targets.

As indicated by the diagrams in Figure 3, MCH treatment reduces nucleotide−gold interactions by displacing nucleotides from surface binding sites, thus promoting end-tethered conformations.[31,32,36] The A15 control in Figure 3c confirms that probes attached via A15 blocks are not completely displaced from gold by the conditions used, as the A15 coated surface remains active toward hybridization after the MCH treatment.

There is little change in the hybridization behavior of the thiolated hairpins after the MCH treatment (Figure 3b). In contrast, the directly adsorbed A15−L5−T15 probes become significantly less available to hybridize with A15 targets (Figure 3a), behaving now more as the folded hairpins with A:T stems in Figure 3b. The end-tethered single-stranded A:T hybrids thus exhibit the stability and symmetric low-yielding hybridization response of folded hairpins, which are not affected by surface interactions (Figure 3b). In contrast, surface interactions both destabilize and break the symmetry of the directly adsorbed single-stranded A:T hybrids, leading to a strongly asymmetric hybridization response; a symmetric low-yielding behavior, however, can be restored for these hybrids by suppressing[31,32,36] DNA−surface interactions via an MCH treatment (Figure 3a).

Single-Stranded P15′:P15 Hybrids. We hypothesize that the effect of the A15 "attachment block" in Figure 1c can be mimicked in a mixed composition sequence by placing a thiol ligand on the P15 terminus of the P15′−T5−P15−SH hairpin, thereby forcing the P15 block to interact with gold by proximity. Indeed, when exposed to the P15′ targets, the P15 blocks of the immobilized hairpins do not produce a detectable hybridization signal (hollow bar in Figure 4b). In contrast, the P15 targets hybridize with P15′ blocks of the immobilized hairpins (black bar in Figure 4b), albeit with a yield lower than that of A15−T20:A15 hybrids in Figure 1c. Without the thiol ligand to break the symmetry, neither arm of the unmodified P15′−T5−P15 hairpins produces statistically significant hybridization signals (hollow black and gray bars in Figure 4a), indicating that *both* asymmetry and destabilization induced by surface interactions are important for producing the asymmetric behavior in Figures 1c, 3a, and 4b.

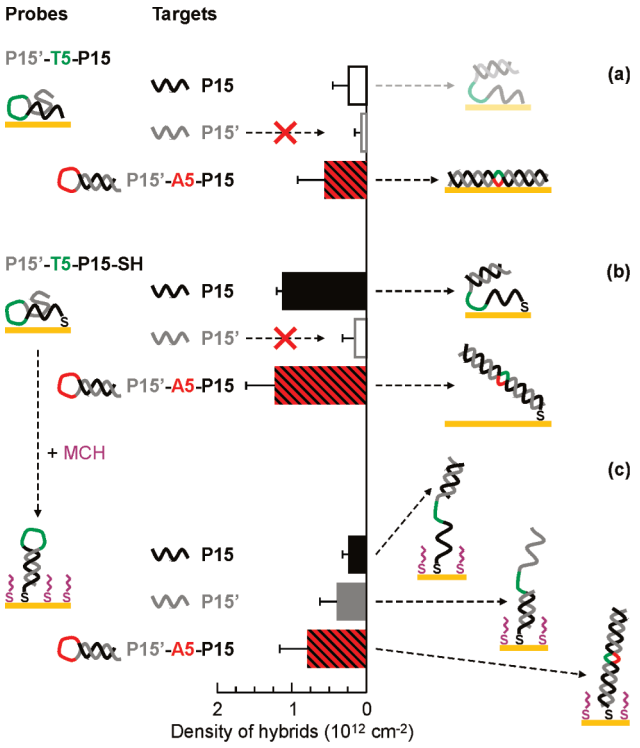

Figure 4. Testing hybridization responses of P15 and P15′ sections of model P15′−T5−P15 and P15′−T5−P15−SH probes immobilized in different conformations. SPR hybridization signals (bar plot) are compared for P15′−T5−P15 (a) and P15′−T5−P15−SH (b) probes as-deposited on bare gold. Hybridization responses of P15′−T5−P15−SH probes are also shown after exposure to 1 mM MCH solution for 5 min (c). Diagrams depict idealized representations of each target-probe pair (black = P15, gray = P15′, green = T15, red = A5) before (diagrams on the left) and after (diagrams on the right) hybridization. Hybridization conditions were the same as those in Figure 1a. Bars are color-coded according to the respective targets (black = P15, gray = P15′, hatched red = P15′−A5−P15); hybridization signals $<2 \times 10^{11}$ cm^{-2} are indicated by crossed-out horizontal arrows; fogged diagrams and hollow bars indicate hybridization signals that are statistically close to the detection limit.

The P15′:P15 hybrids enable us to expand the repertoire of probes and targets in competitive hybridization measurements: in addition to challenging hairpin probes with single-stranded targets (Figures 1 and 3), we also can challenge single-stranded probes (both folded and unfolded) with *hairpin targets* (hatched bars in Figure 4). Notably, P15′−A5−P15 hairpin targets do not produce any detectable hybrids with P15−T5−SH probes (Figure S9, Supporting Information), i.e., a hypothetical reaction that involves opening a solution single-stranded P15′:P15 hairpin hybrid to form an end-tethered *partial* double-stranded hybrid does not proceed. In contrast, full hybrids between complementary P15−A5−P15′ and P15′−T5−P15 sequences offer such a stability advantage that they form not only with end-tethered but also with directly adsorbed hairpin probes (hatched bars in Figure 4).

When P15′−T5−P15−SH hairpin probes are forced into an end-tethered conformation by MCH treatment (Figure 4c),[31,32,36] both arms of the hairpin exhibit the same low and roughly symmetric yields as those observed for end-tethered A:T hairpins in Figure 3b, indicating the increased stability of the hairpin probes in the conformation with reduced surface interactions.

The increased stability of the hairpin probes after the MCH treatment is also manifested in the *reduced* response to the full-complement P15′−A5−P15 hairpin targets: the upright hairpin probes in Figure 4c do not open as readily for hybridization as do the same hairpin probes destabilized by surface interactions in Figure 4b.

DISCUSSION

Our systematic examination of a wide range of DNA hybrids provides evidence for two significant effects of surface interactions on the stability of DNA hybrids. The most general finding is that nucleotide−surface interactions destabilize both single- and double-stranded hybrids. While destabilized relative to their end-tethered counterparts, the directly adsorbed hybrids, however, retain some intramolecular folded structure, which can be disrupted electrostatically or by invasive/competitive hybridization. The second finding is that the products of hybridization reactions with multiple possible outcomes are primarily dictated by the stabilities of initial, transitional, and final hybrids, assuming that the required reactants are present at sufficient concentrations. This finding is particularly encouraging for the ultimate goal of developing design rules for *self-assembling* active and complex DNA structures on surfaces,[2−4] as stability-based rules are already used to design self-assembled DNA-based materials and nanostructures in solutions.[1]

Model A:T Hybrids. We have extensively validated the use of sequences based on (dA) and (dT) blocks to prepare both single- and double-stranded model DNA hybrids on gold surfaces (Figures 1−3). This approach is based on the high affinity of (dA) blocks for gold, which makes them useful as attachment blocks,[10,11,15,20,28] and on the low affinity of (dT) blocks for gold, which makes them into convenient end-tethered hybridization probes.[8,10,11,20,22,28] In agreement with previous reports, we find that end-tethered (T15−SH) probes form hybrids with *higher yield* than do directly adsorbed (A15) probes (Figures 1a and 2)[7,15] and that the resulting end-tethered A15:T15 hybrids are *more stable* than the directly adsorbed ones (Figures 1b and 2).[15] This stability difference persists after extending the hybridization to 2 h (SPR data not shown), making a purely kinetic interpretation of the mechanism unlikely. The destabilization of directly adsorbed A:T hybrids is also consistent with the previously observed nearly complete removal of (dT) strands from A:T hybrids that were formed in solution, adsorbed on gold over ca. 20 h, and rinsed in deionized water before ex situ FTIR measurements.[20]

"Closed" Directly-Adsorbed Hairpins. Upon adsorption on gold, A:T hairpins become destabilized but remain closed, i.e., retain some intramolecular structure, in high ionic strength environment. In SPR measurements, the strongest evidence comes from the failed hybridization attempt of A15−T20 hairpins with T15 targets (green line in Figure 1c). Formation of double-stranded A15:T15 hybrids in Figures 1a and 2b clearly shows that A15 strands interacting with gold do form hybrids, albeit weak ones, with T15 targets. Similarly destabilized hybrids formed by T15 targets with A15 attachment blocks of A15−T5−P15 probes (Figure S4, Supporting Information) further implicate the self-complementary nature of A15−T20 probes in suppressing the equivalent hybridization with T15 targets. The A15−T5−P15 control, in addition, rules out electrostatic repulsion as the main mechanism for suppressing hybridization with T15, as a brush of T5−P15 strands would present a barrier for T15 targets similar to that presented by a brush of T20 strands. Furthermore, the closed hairpin conformation of single-stranded A*m*−T*n* hybrids in NaCl-TE is consistent not only with all the SPR data but also with the quenched fluorescence in Figure S6b (Supporting Information).

The marginal hybridization activity of directly adsorbed P15′−T5−P15 probes in Figure 4a indicates that retaining some of the intramolecular structure upon surface adsorption is not unique to A:T hairpins, but rather is a general property of self-complementary sequences. When the symmetry of the P15′−T5−P15 sequence is broken by adding a thiol ligand, only the P15 block adjacent to the thiol, i.e., the positional equivalent of an A15 attachment block, becomes unavailable for hybridization (Figure 4b). We emphasize that the symmetric and low-yielding hybridization response is the *expected* behavior for stable folded hairpins; all our systematic experiments indicate that *both* the symmetry and stability of hairpin probes must be affected by surface interactions to produce the asymmetric responses associated with "opening" of the respective A15:T15 or P15′:P15 hairpin stems.

Opening Directly-Adsorbed Hairpins. The experiments with double-stranded A:T hybrids introduced two approaches for destabilizing surface-bound hybrids: electrostatic (Figure 1b) and competitive (Figure 2). The results of Figures 1c and d, 3a, and 4b suggest these same approaches can be used to open directly adsorbed hairpins.

Competitive hybridization of A15−T20 with A15 targets readily proceeds in ca. 10 min (Figure 1c), with kinetics characteristic of a hybridization processes. *Displacement* of the adsorbed A15−T20 by the invading A15 target strand can be ruled out as the dominant process based on a kinetic argument. Specifically, the extent and kinetics of disrupting the A15:T15 hybrids in Figure 2b indicate that competitive hybridization with directly adsorbed hybrids has as a low electrostatic barrier. Displacement, however, requires a target strand to penetrate deeply into the DNA film in a process similar to the final phase of A15−T20 immobilization, which is much slower than hybridization and is strongly suppressed under solution conditions similar to those of our hybridization experiments.[8,11,20] Even after 20 h, *coadsorption* rather than displacement is observed for A15−T20 and A15−T5−P15 probes in presence of up to 9:1 molar excess of A7, A15, or A25 diluent strands.[15] Thus any significant displacement of A15−T20 by A15 would require much longer than ca. 10 min observed in Figure 2b. The effective disruption of P15′:P15 hybrids by P15 strands (Figure S3, Supporting Information) also indicates competitive hybridization as the mechanism in common with Figure 2b, rather than displacement that would vary with affinities of A15 and P15 for gold.[15,20]

Upon electrostatic or competitive disruption, the T15 component of a *double-stranded* hybrid leaves the surface (Figures 1a and 2b) while the (dT) arm of a *single-stranded* hybrid remains attached to the surface: as a single (dT) strand extending from the surface in the case of electrostatic disruption or as an end-tethered A:T hybrid in the case of competitive hybridization. The evidence for this conformation change comes from comparing the formation and stability of the A15−T20:A15 hybrids in Figures 1c and d to those of the end-tethered A15:T15−SH hybrids in Figures 1a and b. The similar hybridization yield and stability in both cases are consistent with observing end-tethered hybrids in both systems.

Both the electrostatic and competitive mechanisms are tested more directly in Figure S6 (Supporting Information), where increased fluorescence is observed after exposing A15−T30*

Scheme 1. Relative Scale of Stability for Surface-Immobilized DNA Hybrids

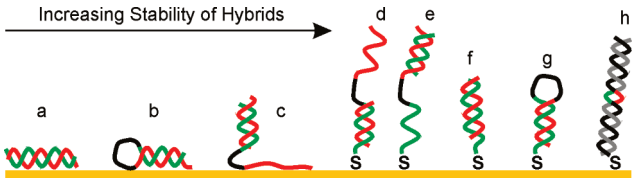

probes to either deionized water or complementary A15 targets. Fluorescence observed in both cases indicates that the labeled (dT) arm is extended away from the gold surface.[13,31,32] The change from negative to positive dichroism in NEXAFS for A5−T15 probes after hybridization with A15 targets (Figure S8, Supporting Information) also indicates that the resulting hybrids are extended away from the surface.

Relative Stabilities of DNA Hybrids. The combined results of all the competitive experiments in Figures 1−4 indicate that the products of hybridization reactions with multiple possible outcomes are primarily dictated by the stabilities of initial, transitional, and final hybrids. A qualitative relative stability scale can be derived from our observations (Scheme 1).

Double-stranded directly adsorbed hybrids (Scheme 1a) have the lowest stability, followed by single-stranded directly adsorbed hybrids (Scheme 1b). The somewhat higher stability of the latter is indicated by the failed reactions in Figures 1c, 3a (top), and 4a and b where a pre-existing single-stranded hybrid would be replaced with a double-stranded equivalent. Double-stranded end-tethered hybrids (Scheme 1c−f) are more stable than any directly adsorbed hybrids (Scheme 1a,b), as indicated by direct measurements in Figures 1b and S2 (Supporting Information) and by all reactions where adsorbed hairpins open to form end-tethered hybrids: Figures 1c (red line), 3a (top), S6c, and S9a (Supporting Information). In contrast with a previous report for longer probe sequences,[18] no significant difference is observed in our study between *partial* hybrids (Scheme 1d,e) formed with upper and lower portions of end-tethered probe sequences (Figures 3b and 4c). Single-stranded end-tethered hybrids (Scheme 1g) are more stable than their double-stranded counterparts (Scheme 1f), as indicated by suppressed yields in all reactions where end-tethered hairpins are challenged by solution targets: Figures 3a (MCH) and b and 4c. Finally, double-stranded hybrids formed by end-tethered hairpins and their full complements (Scheme 1h) are the longest and thus the most stable.

CONCLUSIONS

We have systematically analyzed the effects of surface interactions on the stability of DNA hybrids immobilized on gold in different conformations. Using a combination of complementary SPR, XPS, NEXAFS, and fluorescence measurements we have established that both single- and double-stranded DNA hybrids are destabilized by surface interactions and have derived a qualitative scale of relative stabilities for the different conformations of hybrids on gold (Scheme 1). Self-complementary A*m*−T*n* sequences have proven to be versatile models for elucidating the properties of single-stranded hybrids and revealed general stability trends, as demonstrated in complementary experiments with mixed-composition hybrids.

We find that the stability, structure, and resulting hybridization activity of single-stranded probes directly adsorbed on gold can be predictably controlled using three approaches: adjusting ionic strength of the buffer solution (electrostatic destabilization), introducing invasive or competitive solution targets (competitive destabilization), and controlling nucleotide−surface interactions (via composition, thiol placement, or MCH backfill). Following these approaches, single-stranded hybrids can be designed to produce asymmetric hybridization responses that are determined by external stimuli (e.g., solution targets or ionic strength), i.e., such surface-bound hairpins can act as switches or other active structures similar to those used in DNA-based motors and walkers.[1,3] Significantly, the outcomes of hybridization reactions involving structured probes or targets are primarily dictated by the stabilities of initial, transitional, and final hybrids. Stability trends, such as those established in this work, thus offer a promising pathway toward the ultimate goal of developing design rules for *self-assembling* active and complex DNA structures *on surfaces*,[2−4] as similar principles are used successfully to design and produce self-assembled DNA-based materials and nanostructures in solutions.[1]

ASSOCIATED CONTENT

Supporting Information. Materials and methods; negative control for hybridization with A15 probes; formation and stability of mixed-composition P15′:P15 hybrids; XPS N 1s data for A15−T20; fluorescence measurements; NEXAFS measurements. This material is available free of charge via the Internet at http://pubs.acs.org.

AUTHOR INFORMATION

Corresponding Author

*E-mail: dpetrovykh@inl.int (D.Y.P.), opdahl.aric@uwlax.edu (A.O.).

Present Address

▽International Iberian Nanotechnology Laboratory, Avenida Mestre José Veiga, 4715−310 Braga, Portugal.

ACKNOWLEDGMENT

Research at UW−La Crosse was supported by an award from Research Corporation. D.Y.P. was supported by the Air Force Office of Scientific Research. C.H. was supported by a US-NSF Graduate Research Fellowship. C.H., J.Z., P.K., and M.Z. received funding from DFG (ZH 63/9-3 and 10-1) and the European Community's Seventh Framework Programme (FP7/2007-2013) under grant agreement No. 226716. A.O. thanks B. P. Nelson for advice on SPR measurements. D.Y.P. thanks T. D. Clark (NRL) for stimulating discussions of DNA properties. C.H., J.Z., P.K., and M.Z. thank M. Grunze (Heidelberg) for research support and helpful discussions.

REFERENCES

(1) Seeman, N. C. *Annu. Rev. Biochem.* **2010**, *79*, 65–87.
(2) Rothemund, P. W. K. *Nature* **2006**, *440*, 297–302.
(3) Omabegho, T.; Sha, R.; Seeman, N. C. *Science* **2009**, *324*, 67–71.
(4) Kershner, R. J.; Bozano, L. D.; Micheel, C. M.; Hung, A. M.; Fornof, A. R.; Cha, J. N.; Rettner, C. T.; Bersani, M.; Frommer, J.; Rothemund, P. W. K.; Wallraff, G. M. *Nat. Nanotechnol.* **2009**, *4*, 557–561.
(5) Du, H.; Strohsahl, C. M.; Camera, J.; Miller, B. L.; Krauss, T. D. *J. Am. Chem. Soc.* **2005**, *127*, 7932–7940.
(6) Brewood, G. P.; Rangineni, Y.; Fish, D. J.; Bhandiwad, A. S.; Evans, D. R.; Solanki, R.; Benight, A. S. *Nucleic Acids Res.* **2008**, *36*, e98.

(7) Gong, P.; Lee, C. Y.; Gamble, L. J.; Castner, D. G.; Grainger, D. W. *Anal. Chem.* **2006**, *78*, 3326–3334.
(8) Petrovykh, D. Y.; Kimura-Suda, H.; Whitman, L. J.; Tarlov, M. J. *J. Am. Chem. Soc.* **2003**, *125*, 5219–5226.
(9) Herne, T. M.; Tarlov, M. J. *J. Am. Chem. Soc.* **1997**, *119*, 8916–8920.
(10) Wolf, L. K.; Gao, Y.; Georgiadis, R. M. *Langmuir* **2004**, *20*, 3357–3361.
(11) Opdahl, A.; Petrovykh, D. Y.; Kimura-Suda, H.; Tarlov, M. J.; Whitman, L. J. *Proc. Natl. Acad. Sci. U.S.A.* **2007**, *104*, 9–14.
(12) Levicky, R.; Herne, T. M.; Tarlov, M. J.; Satija, S. K. *J. Am. Chem. Soc.* **1998**, *120*, 9787–9792.
(13) Lee, C. Y.; Gong, P.; Harbers, G. M.; Grainger, D. W.; Castner, D. G.; Gamble, L. J. *Anal. Chem.* **2006**, *78*, 3316–3325.
(14) Lee, C. Y.; Nguyen, P. C. T.; Grainger, D. W.; Gamble, L. J.; Castner, D. G. *Anal. Chem.* **2007**, *79*, 4390–4400.
(15) Schreiner, S. M.; Shudy, D. F.; Hatch, A. L.; Opdahl, A.; Whitman, L. J.; Petrovykh, D. Y. *Anal. Chem.* **2010**, *82*, 2803–2810.
(16) Fish, D. J.; Horne, M. T.; Brewood, G. P.; Goodarzi, J. P.; Alemayehu, S.; Bhandiwad, A.; Searles, R. P.; Benight, A. S. *Nucleic Acids Res.* **2007**, *35*, 7197–7208.
(17) Gao, Y.; Wolf, L. K.; Georgiadis, R. M. *Nucleic Acids Res.* **2006**, *34*, 3370–3377.
(18) Poulsen, L.; Soe, M. J.; Snakenborg, D.; Moller, L. B.; Dufva, M. *Nucleic Acids Res.* **2008**, *36*, e132.
(19) Levicky, R.; Horgan, A. *Trends Biotechnol.* **2005**, *23*, 143–149.
(20) Kimura-Suda, H.; Petrovykh, D. Y.; Tarlov, M. J.; Whitman, L. J. *J. Am. Chem. Soc.* **2003**, *125*, 9014–9015.
(21) Petrovykh, D. Y.; Kimura-Suda, H.; Tarlov, M. J.; Whitman, L. J. *Langmuir* **2004**, *20*, 429–440.
(22) Petrovykh, D. Y.; Pérez-Dieste, V.; Opdahl, A.; Kimura-Suda, H.; Sullivan, J. M.; Tarlov, M. J.; Himpsel, F. J.; Whitman, L. J. *J. Am. Chem. Soc.* **2006**, *128*, 2–3.
(23) Jung, L. S.; Campbell, C. T.; Chinowsky, T. M.; Mar, M. N.; Yee, S. S. *Langmuir* **1998**, *14*, 5636–5648.
(24) Sale, W. S.; Howard, D. R. *Methods Cell Biol.* **1995**, *47*, 257–262.
(25) Batson, P. E. *Phys. Rev. B* **1993**, *48*, 2608–2610.
(26) Östblom, M.; Liedberg, B.; Demers, L. M.; Mirkin, C. A. *J. Phys. Chem. B* **2005**, *109*, 15150–15160.
(27) Storhoff, J. J.; Elghanian, R.; Mirkin, C. A.; Letsinger, R. L. *Langmuir* **2002**, *18*, 6666–6670.
(28) Samuel, N. T.; Lee, C. Y.; Gamble, L. J.; Fischer, D. A.; Castner, D. G. *J. Electron Spectrosc. Relat. Phenom.* **2006**, *152*, 134–142.
(29) Ray, S. G.; Cohen, H.; Naaman, R.; Rabin, Y. *J. Am. Chem. Soc.* **2005**, *127*, 17138–17139.
(30) Demers, L. M.; Mirkin, C. A.; Mucic, R. C.; Reynolds, R. A.; Letsinger, R. L.; Elghanian, R.; Viswanadham, G. *Anal. Chem.* **2000**, *72*, 5535–5541.
(31) Rant, U.; Arinaga, K.; Fujita, S.; Yokoyama, N.; Abstreiter, G.; Tornow, M. *Langmuir* **2004**, *20*, 10086–10092.
(32) Arinaga, K.; Rant, U.; Tornow, M.; Fujita, S.; Abstreiter, G.; Yokoyama, N. *Langmuir* **2006**, *22*, 5560–5562.
(33) Ballav, N.; Koelsch, P.; Zharnikov, M. *J. Phys. Chem. C* **2009**, *113*, 18312–18320.
(34) Stöhr, J.; Outka, D. A. *Phys. Rev. B* **1987**, *36*, 7891–7905.
(35) Zubavichus, Y.; Shaporenko, A.; Korolkov, V.; Grunze, M.; Zharnikov, M. *J. Phys. Chem. B* **2008**, *112*, 13711–13716.
(36) Park, S.; Brown, K. A.; Hamad-Schifferli, K. *Nano Lett.* **2004**, *4*, 1925–1929.

Supporting Information

Impact of DNA-Surface Interactions on the Stability of DNA Hybrids

Sarah M. Schreiner,[†] Anna L. Hatch,[†] David F. Shudy,[†] David R. Howard,[‡] Caitlin Howell,[§,∥] Jianli Zhao,[∥] Patrick Koelsch,[§,∥] Michael Zharnikov,[∥] Dmitri Y. Petrovykh,*[,⊥] Aric Opdahl*[,†]

[†]*Department of Chemistry, University of Wisconsin—La Crosse, La Crosse, WI 54601, USA;* [‡]*Department of Biology, University of Wisconsin—La Crosse, La Crosse, WI 54601, USA;* [§]*Institute of Toxicology and Genetics, Karlsruhe Institute of Technology, Hermann-von-Helmholtz-Platz 1, 76344 Eggenstein-Leopoldshafen, Germany;* [∥]*Angewandte Physikalische Chemie, Universität Heidelberg, Im Neuenheimer Feld 253, 69120 Heidelberg, Germany;* [⊥]*Department of Physics, University of Maryland, College Park, MD 20742, USA*

**E-mail: opdahl.aric@uwlax.edu, dpetrovykh@inl.int*

MATERIALS AND METHODS

Materials. Custom oligonucleotides, purchased from commercial DNA vendors, are written here in the 5' to 3' direction. Sequences used in hybridization experiments included a 15-nucleotide adenine homo-oligo (A15); a 15-nucleotide thymine homo-oligo (T15); a mixed sequence of 15 nucleotides (5'-CAATGCAGATACACT-3', denoted P15) and its full complement (5'-AGTGTATCTGCATTG-3', denoted P15'). These sequences were incorporated as components (blocks) into longer self-complementary DNA strands, including A15–T20; P15–T5–P15'; and P15'–A5–P15. Oligos denoted with –SH have a 3' thiol modification and were used in the as-received asymmetric disulfide form, i.e., without removing the –S–$(CH_2)_3$–OH protecting group from the 3' end (Refs 8, 21). The sequence denoted A15–T30* is labeled with fluorescent TAMRA at the 3' end. Buffers denoted NaCl-TE and $CaCl_2$-TE contained 1 M NaCl or $CaCl_2$, respectively, 1×TE (10 mM Tris·HCl, 1 mM EDTA), and were adjusted to pH 7 with HCl. The 1-mercapto-6-hexanol (MCH) was purchased from Fisher Scientific. The 1-mercapto-11-undecyl triethylene glycol (PEG–SH), was obtained from Asemblon (Redmond, WA).

Gold Substrates. Commercial SPR glass slides coated with ca. 47 nm of gold were used for SPR analysis. Substrates for XPS and NESAFS analysis were Si(100) wafers coated with 5 nm of Ti followed by 100 nm of Au. Gold surfaces for SPR, XPS, and confocal microscopy experiments were cleaned with piranha solution [70% H_2SO_4 30% H_2O_2 (30% H_2O_2 in H_2O)] and rinsed thoroughly with deionized water (18.2 MΩ) immediately prior to use. *Caution*: Piranha solution is extremely oxidizing, reacts violently with organics, and should be stored in loosely covered containers to avoid pressure buildup.

DNA Immobilization. For probes without thiol modifications, DNA immobilization followed a standard procedure that yields high surface densities (Refs 11, 15): clean gold surfaces were incubated at 35 °C for 20 h with DNA solutions (4 μM DNA in $CaCl_2$-TE buffer). After immobilization, each sample was rinsed sequentially with deionized water, NaCl-TE buffer, 0.1 M NaOH, and deionized water, before drying under flowing nitrogen. This four-step rinse procedure removes calcium ions and weakly bound DNA from the surface. For probes with thiol functionality, immobilization from 4 μM DNA solutions in NaCl-TE buffer for ca. 2 h at room temperature was used to produce probe surface densities comparable to those of unmodified probe sequences. Hybridization solutions contained 4 μM target DNA in NaCl-TE buffer at room temperature.

Patterned Samples for Fluorescence Measurements. Simple DNA arrays with 500×500 μm^2 square gold regions surrounded by a monolayer of PEG–SH were prepared by soaking piranha-cleaned SPR sensors for 20 h in ethanolic 1 mM PEG–SH (Asemblon, Redmond, WA), rinsing, drying, covering with a mask, and treating for 2 h under a 500 W UV mercury arc lamp equipped with a liquid IR filter. This exposure produced an array of 500×500 μm^2 squares of UV-cleaned gold separated by PEG–SH regions. The patterned SPR sensors were rinsed with ethanol and buffer solution prior to DNA probe immobilization. Fluorescent A15–T30* probes were then immobilized in the clean gold regions following the procedure described above.

Samples for NEXAFS Measurements. Gold surfaces for NEXAFS experiments were cleaned for 2.5 h in a commercial UV/ozone cleaner. A5–T15, A15, and T6–SH probes were immobilized on clean gold substrates at 37 °C for 40 h from 3 μM DNA solutions in $CaCl_2$-TE buffer. Samples were then washed under flowing deionized water for ca. 1 min and dried under flowing nitrogen. Some of the freshly rinsed A5–T15 samples were immersed into a 3 μM solution of A15 targets in NaCl-TE buffer for 8 h at room temperature. Samples were then rinsed under flowing NaCl-TE buffer for ca. 1 min, *briefly dipped* into deionized water to remove excess salts, and dried under flowing nitrogen. The samples were stored under inert gas atmosphere in glass containers until they were transferred into vacuum for measurements at the synchrotron radiation facility.

Surface Plasmon Resonance (SPR). DNA immobilization and hybridization were measured *in situ* using an SPR imaging system (GWC, Madison, WI) as described previously (Ref 15). Our quantitative analysis followed established methods outlined by Jung *et al*. (Refs 15, 23). We assumed the effective "bulk" values of DNA density (1.7 g/cm^3) and refractive index (1.7) that are commonly used as parameters for SPR quantification (Ref 15).

To obtain quantitative measurements during the stringency rinse experiments (Ref 15), SPR sensors prehybridized in 1 M NaCl were rinsed with successively lower ionic strength buffer solutions for 4 min. After each rinse step, a blank 1 M NaCl buffer was flowed through the liquid cell and the change in reflected light was recorded. Returning to the original 1 M NaCl buffer solution after each step produces measured changes in light intensity that can be directly attributed to DNA loss, thus eliminating the need to account for differences in refractive indexes of the rinse buffers (Ref 15).

X-ray Photoelectron Spectroscopy (XPS). Quantitative XPS analysis was used to measure surface densities of DNA probes *ex situ* for several witness samples, which were prepared similarly to samples used in SPR and NEXAFS measurements. XPS was performed in a system equipped with a monochromatic Al Kα source, a magnetic electron lens, and a hemispherical electron energy analyzer; data were analyzed using methods previously described in Refs 11 and 21.

Fluorescence Microscopy. Laser-scanning confocal fluorescence microscopy images were obtained using a Nikon CS1 confocal system. Images were obtained using a 40× oil 1.3 NA objective, 561 nm diode pumped solid state laser, and PMT detection. A simple liquid cell was constructed using double-sided tape to form a channel between the gold coated slide and a

glass coverslip (Ref 24). Image brightness and contrast were adjusted for clarity of presentation.

NEXAFS. Near-edge x-ray absorption fine structure (NEXAFS) spectroscopy measurements were made on beamline D1011 at the MAX II storage ring at the MAX-lab synchrotron radiation facility in Lund, Sweden. The spectra at the nitrogen K-edge were acquired under linearly polarized light (ca. 95% polarization) in the partial electron yield mode with retarding voltage of -300 V. The energy resolution was <100 meV; the energy scale was referenced to the most intense π* resonance of highly oriented pyrolytic graphite at 285.38 eV (Ref 25). The incidence angle of the x-rays was varied from 90° (**E**-vector in the surface plane) to 20° in steps of 10°–20° to monitor the orientation and ordering of nucleobases within the DNA films.

The raw NEXAFS spectra were normalized to the incident photon flux by division through a spectrum of a clean, freshly sputtered gold sample. The spectra then were reduced to the standard form by subtracting linear pre-edge background and normalizing to the unity edge jump (determined by a nearly horizontal plateau 40–50 eV above the absorption edge).

RESULTS

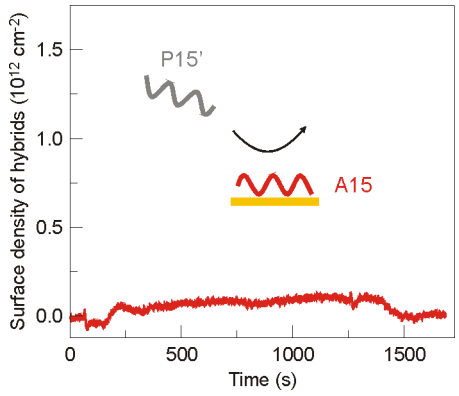

Figure S1. Typical SPR signal for an attempted hybridization of non-complementary target with A15 probes immobilized on gold. A clean SPR sensor was pre-incubated to produce saturation surface density of ca. 1.3×10^{13} cm^{-2} of unmodified A15 probes on gold (data for A15 immobilization not shown), then exposed for ca. 20 min to 4 μM solution of a P15' target in 1 M NaCl-TE buffer, followed by a rinse for ca. 5 min in blank buffer. Note that the signal returned to baseline after the buffer rinse, indicating no significant hybridization. Diagram depicts idealized representations of P15' targets (gray) and A15 probes (red). The target sequence denoted P15' was the same as in Figure S2.

Hybrids of Mixed-Composition Sequences. We test the generality of the trends observed for A:T hybrids by performing experiments parallel to those in Figures 1 and 2 for hybrids formed by complementary P15 and P15′ sequences that have mixed nucleotide compositions. In contrast to the A:T models, in which the high affinity of (dA) blocks for gold unambiguously defined the component of a hybrid that was strongly interacting with the surface, no such *a priori* asymmetry can be expected between P15 and P15′ sequences. Nevertheless, gold surfaces functionalized with unmodified P15 and P15–T5–SH probes behave in hybridization experiments with P15′ targets (Figure S2a) in a manner similar to the directly-adsorbed A15 and end-tethered T15–SH probes, respectively, in Figure 1a. Furthermore, the stability of the resulting P15′:P15 and P15′:P15–T5–SH hybrids (Figure S2b) qualitatively follows the trends of the directly-adsorbed and end-tethered hybrids in Figure 1b, indicating that the range of properties expected for P15′:P15 hybrids in different conformations is comparable to that observed for the model A:T hybrids in Figures 1 and 2.

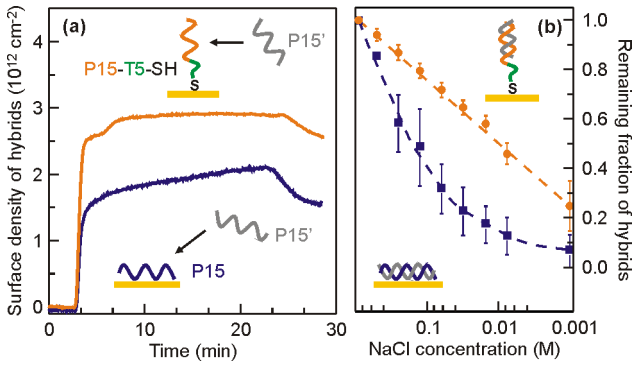

Figure S2. Formation and stability of hybrids formed with mixed-composition probes in directly-adsorbed and end-tethered conformations. Diagrams depict idealized representations of each target–probe pair (orange = P15–T5–SH and blue = P15 probes; gray = P15' target) before and after hybridization (a) and during melting (b). The line and symbol colors in the data plots correspond to the color-coding of the respective probes: end-tethered P15–T5–SH (orange) or directly-adsorbed P15 (blue). In each hybridization experiment (a), the sensor was exposed for ca. 20 min to 4 μM solution of a target in 1 M NaCl-TE buffer, followed by a rinse for ca. 5 min in blank buffer to remove any weakly bound DNA targets. The stringency rinse profiles in (b) were obtained by exposing *prehybridized* SPR sensors to solutions of successively lower NaCl concentration and monitoring the number of hybrids remaining on the surface. The probe sequence denoted P15 was 5'-CAATGCAGATACACT-3'; complementary target denoted P15' was 5'-AGTGTATCTGCATTG-3'. Error bars in panel (b) represent variation among replicate samples.

Relative Stabilities of Double-Stranded P15′:P15 Hybrids. The trends between relative stabilities of directly-adsorbed and end-tethered P15′:P15 hybrids in competitive experiments parallel those observed in Figure 2 for the A:T hybrids. The comparison between the two conformations in Figure S3 is more direct than that in Figure 2 because a comparable density (ca. 1.0×10^{13} cm^{-2} measured by SPR) of the *same* P15 sequence is used in both initial probe surfaces (P15 and P15–T5–SH in Figure S3). Compared to T15–SH probes in Figure 2, the yield for P15–T5–SH in Figure S3 is lower, most likely because the P15–T5–SH strands immobilized at ca. 30–40% lower density produce fewer upright end-tethered probes (Refs 8, 21, 22).

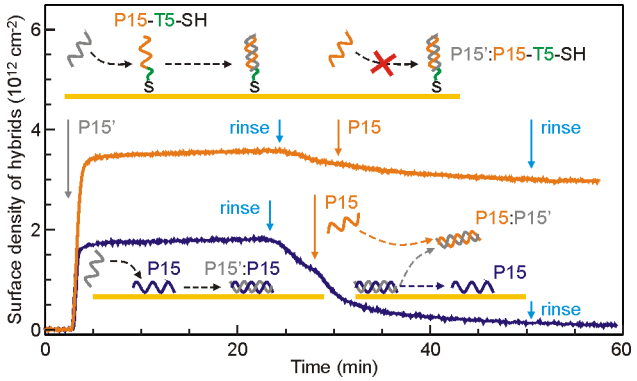

Figure S3. Different conformations of double-stranded P15:P15′ hybrids subjected to stability challenges by invasive hybridization. Diagrams depict idealized representations of each target-probe pair (orange = P15, gray = P15′, dark blue = P15 probes in directly-adsorbed conformation) through two hybridization attempts/challenges. The line colors of the data plots correspond to the respective probes: orange for end-tethered P15–T5–SH and dark blue for directly-adsorbed P15. In each experiment, the SPR sensor was sequentially exposed to: P15′ target (vertical gray arrow at ca. 3 min); blank 1 M NaCl-TE buffer (cyan arrows at ca. 23–25 min); P15 target (orange arrows at ca. 28–30 min); and the final rinse in blank buffer (cyan arrows after ca. 50 min). Hybridization conditions were the same as those in Figure S2.

When exposed to the complementary P15′ targets (vertical gray arrow at ca. 3 min in Figure S3), the end-tethered P15–T5–SH probes (orange in Figure S3) show higher hybridization activity compared to that of the directly-adsorbed P15 probes (dark blue in Figure S3). When a competitive solution of P15 targets is introduced (orange arrows at ca. 28–30 min in Figure S3), the end-tethered P15′:P15–T5–SH hybrids are barely affected, while the directly-adsorbed P15′:P15 hybrids are nearly completely disrupted (dark blue line after ca. 50 min in Figure S3).

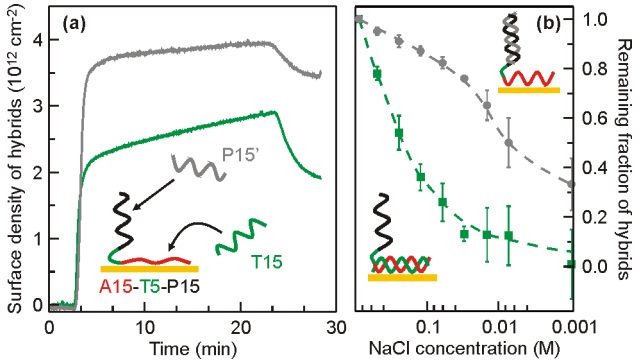

Figure S4. Formation and stability of hybrids formed with probes containing P15 and A15 sequences. Diagrams depict idealized representations of L-shape probes and their hybrids (red = adenine, green = thymine, black = P15 probe, grey = P15' target) before (a) and after (b) hybridization. The line and symbol colors in the data plots correspond to the color-coding of the respective targets: P15' (gray) or T15 (green); e.g., in (a), the green curve corresponds to A15–T5–P15+T15. Surface density of A15–T5–P15 probes was ca. 1.3×10^{13} cm^{-2}. Experimental conditions, P15 and P15' sequences were the same as in Figure S2. Error bars in (b) represent variation among replicate samples.

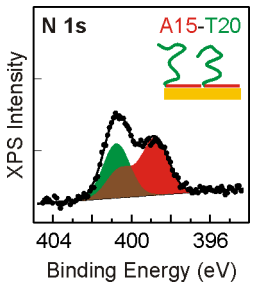

Figure S5. XPS data in N 1s region for A15–T20 model probes immobilized on gold. Immobilization was performed for 20 h from a 4 μM DNA solution in 1 M $CaCl_2$-TE buffer at 35 °C. The characteristic N 1s "singlet" and "doublet" envelopes for thymine and adenine are shaded in green and red, respectively. Each adenine and thymine nucleobase contains 5 and 2 nitrogen atoms, respectively, resulting in a proportionately stronger adenine signal. The surface density of A15–T20 probes calculated from XPS data for this sample is $1.45\pm0.10\times10^{13}$ cm^{-2}.

Single-Stranded A:T Hybrids: Fluorescence Microscopy. We use fluorescently labeled A15–T30* (* denotes TAMRA label) to take advantage of distance-dependent quenching for fluorescent molecules placed in proximity to a gold surface (Refs 13, 31, 32). Specifically for A15–T30*, such fluorescence measurements allow us to track the proximity of the TAMRA-labeled 3′ terminal to the gold surface. The longer T30 block, rather than T20 in Figure 1c, provides sufficient extension away from the gold surface for fluorescence enhancement in the putative L-shape conformation (Refs 31, 32).

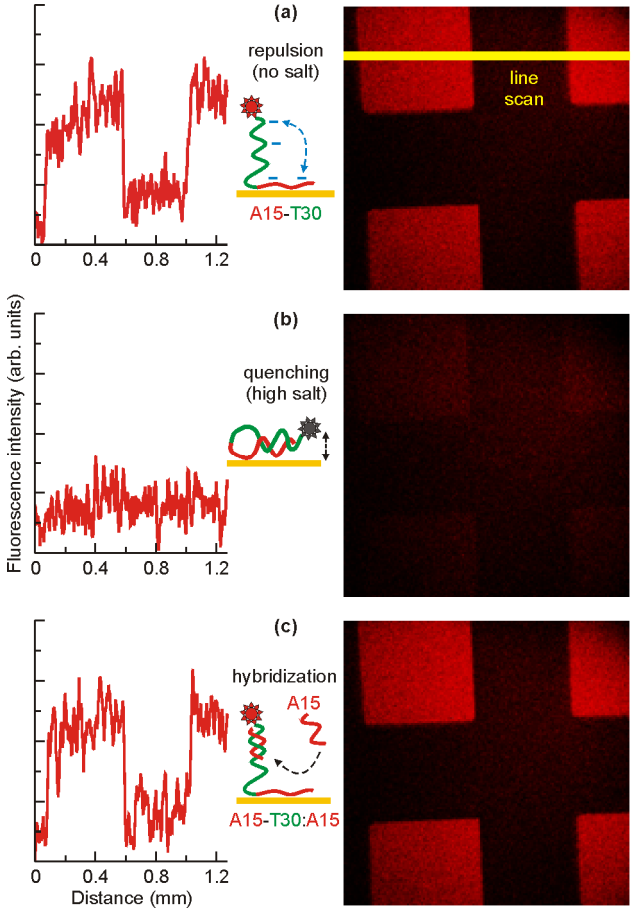

Figure S6. Conformational changes for fluorescently-labeled A15–T30* probes monitored by laser scanning confocal microscopy. Photopatterned surfaces contain 500×500 μm^2 square regions of model A15–T30* probes immobilized on clean gold surrounded by the background of gold backfilled with PEG–SH. Fluorescence images and representative line scans are shown for samples in contact with deionized water (a), 1 M NaCl-TE buffer (b), and 4 μM solution of A15 target in 1 M NaCl-TE (c). Diagrams depict idealized representations of model A15–T30* probes under the respective solution conditions (red lines = adenine, green lines = thymine); red and dark gray star-shaped polygons represent the fluorescent and quenched states of the TAMRA label, respectively; cyan "-" signs and arrow in (a) indicate electrostatic repulsion between the two sections of A15–T30*.

Figure S6 shows fluorescence images obtained from gold surfaces functionalized with directly-adsorbed A15–T30* hairpins and then placed in contact with three different solutions. Visual contrast was achieved by patterning 500×500 μm^2 square regions of fluorescent A15–T30* in a background of non-fluorescent self-assembled monolayer (SAM) of PEG–SH (Ref 15). In 1 M NaCl-TE buffer, no fluorescence is observed from the A15–T30* regions, relative to the surrounding PEG–SH regions (Figure S6b). The faint background is attributed to incomplete filtering of the excitation source and was observed in control experiments using uniform SAMs of PEG–SH on gold.

When the NaCl-TE buffer is replaced with deionized water, the fluorescence signal from the A15–T30* regions of the surface increases significantly (Figure S6a). The fluorescence enhancement and quenching is reversible over several cycles of switching between deionized water and 1 M NaCl-TE. In control experiments, fluorescence signal from TAMRA solutions changed by <20% as a function of their ionic strength and pH (Figure S7).

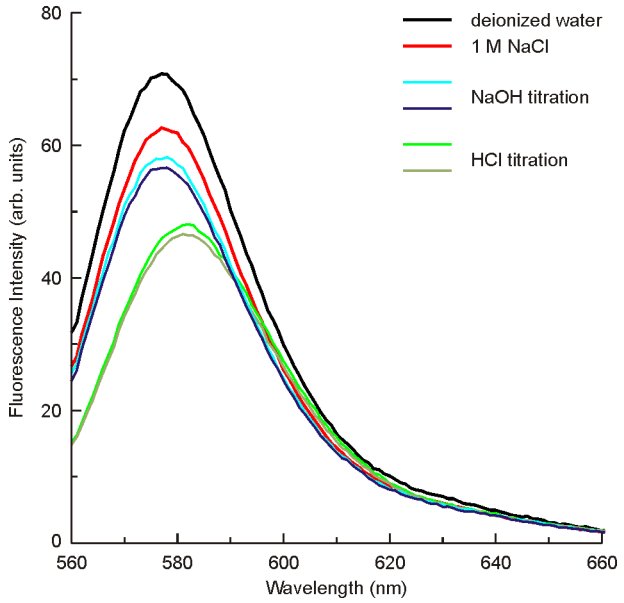

Figure S7. Variation of TAMRA fluorescence intensity with solution conditions. Changes in ionic strength or solution pH resulted in <20% variation of the TAMRA fluorescence relative to the reference intensity in 1 M NaCl.

Under the high-salt conditions of the 1 M NaCl-TE buffer, enhancement of the fluorescence signal from the A15–T30* regions is observed upon addition of A15 target (Figure S6c). This enhancement of the fluorescence signal is quantitatively similar to that observed in deionized water (cf. Figures S6a) and is also reversible. When the hybridized surface is rinsed with a denaturing 0.1 M NaOH solution and subsequently placed in 1 M NaCl-TE, the A15–T30* regions darken to the levels of Figure S6b.

Single-Stranded A:T Hybrids: NEXAFS. For label-free evaluation of hybrids formed with A*n*–T*m* probes, we used NEXAFS to characterize hybrids formed with A5–T15 probes. The short A5 block provides stable attachment for A5–T*m* probes on gold (Refs 11, 15) and reduces ambiguity of the spectral features at the nitrogen K-edge: (dA) spectral contribution is minimized before hybridization and maximized for putative A5–T15:A15 hybrids.

As previously demonstrated for model DNA films on gold (Refs 13, 22, 28, 33), NEXAFS features at the K-edge of nitrogen provide useful information about the orientation and ordering of surface-immobilized DNA molecules. NEXAFS takes advantage of linearly-polarized synchrotron x-rays to measure the variation of NEXAFS intensity as a function of the x-ray incident angle with respect to the surface (and the molecular orbitals in any film on that surface). NEXAFS selection rules (Ref 34) dictate that spectra acquired at the "magic" angle of incidence (55°) are insensitive to molecular orientation and thus characteristic of the chemical identity of samples (Figure S8a). In spectra acquired at normal (90°) and grazing (20°) angles, the contributions from π* orbitals oriented parallel and normal to the surface, respectively, are enhanced. In DNA, N π* orbitals are exclusively contained in nucleobases and are normal to the aromatic rings (Ref 22). The N π* signal is, therefore, enhanced at grazing incidence for roughly upright DNA strands; conversely, the signal is enhanced at normal incidence for directly-adsorbed (in-plane oriented) DNA strands. Plotting the difference between the spectra acquired at 20° and 90° angles of incidence conveniently visualizes the NEXAFS linear dichroism for DNA, whereby positive features indicate DNA molecules extended away from the surface (Figure S8b).

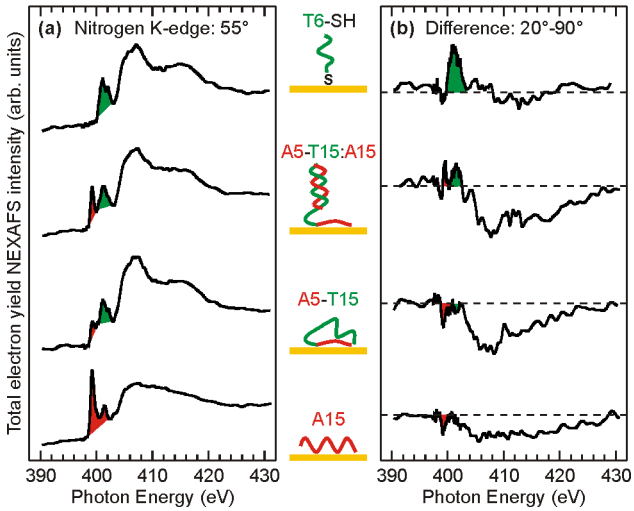

Figure S8. Nitrogen K-edge NEXAFS spectral signatures and molecular conformations in model DNA films on gold. Panels show spectra acquired with incident x-rays at 55° (a) and the difference between spectra acquired with incident x-rays at 20° and 90° (b). The spectra and diagrams in the central two rows are for a film of model A5–T15 probes (as-deposited from 3 μM solution in $CaCl_2$-TE buffer) and for a film, denoted A5–T15:A15, of the A5–T15 probes after hybridization in 3 μM solution of A15 targets in NaCl-TE buffer. Spectra for T6–SH and A15 films deposited from 3 μM solutions in $CaCl_2$-TE are shown as references for the resonance lineshapes characteristic of the respective homo-oligonucleotides (a) and the characteristic polarities of linear dichroism for upright (T6–SH) and in-plane (A15) orientations of DNA strands (b). The most pronounced features characteristic of A and T nucleobases are indicated by red and green shading, respectively. Spectra are offset for clarity, zero lines in the difference spectra are indicated by horizontal dashed lines in (b). After deposition, A15, T6–SH, and A5–T15 samples were rinsed in deionized water for ca. 1 min, while A5–T15:A15 sample was only briefly dipped into deionized water to minimize destabilization of A:T hybrids similar to that in Figure 1d.

The nitrogen K-edge NEXAFS spectra are presented in Figure S8 for four model DNA films: A5–T15 probes before and after hybridization with A15 targets, and T6–SH and A15 references. The nitrogen K-edge spectra in Figure S8a have the overall shapes typical for NEXAFS spectra of DNA films (Refs 13, 22, 28, 33), in particular, all the spectra exhibit π* resonances in the pre-edge region. The distinct lineshapes and positions of the characteristic π* resonances for adenine and thymine (shaded red and green in Figure S8, respectively) are clearly observed in the reference spectra of A15 and T6–SH and are consistent with spectra reported in the literature for similar DNA films (Refs 22, 28, 33, 35). In contrast to a complete overlap of (dA) and (dT) features in XPS N 1s data (cf. Figure S5), the separation of the most intense components of π* resonances for (dA) and (dT) allows for a qualitative assignment of the main features in the spectra of A5–T15:A15 and A5–T15 (indicated by shading in Figure S8).

A change from negative to positive dichroism is observed between spectra of A5–T15 and A5–T15:A15 in Figure S8b, as would be expected if the initial in-plane orientation of the T15 block changes to one extended away from the surface upon hybridization with an A15 target (which also is extended away from the surface as part of the same hybrid). We note that the negative dichroism observed for the A5 block of A5–T15 is consistent with the presumed in-plane orientation of the A5 attachment block, whereas after hybridization with the longer A15 targets, the (dA) component of the spectra is significantly increased and presumably dominated by the signal from the

hybrids. In agreement with the inferences from Figures 1 and 2 and from previous studies (Refs 8, 11, 20, 22, 28), dichroism signal is negative for A15 and positive for T6–SH controls, indicating in-plane and upright orientations of the respective DNA strands.

Observing the expected change in both composition (Figure S8a) and orientation (Figure S8b) between the spectra for A5–T15 and A5–T15:A15 samples is particularly significant, because the rinsing and drying procedures required before *ex situ* NEXAFS measurements can potentially interfere with the conformation and stability of any hybrids formed in solution. At least two factors likely contributed to preserving the A5–T15:A15 hybrids during an intentionally brief dip-rinse applied to the sample after hybridization. First, the data in Figures 1–2 indicate that all the end-tethered variants of A15:T15 hybrids significantly denature only after more than a few seconds (e.g., 4 min for each step in Figures 1b and 1d) in low ionic strength solutions. Second, the enhanced fluorescence in Figure S6c indicates a strong electrostatic repulsion between even partial A:T hybrids and the attachment A*n* blocks of A*n*–T*m* probes; a similar repulsion can be expected to support the roughly upright orientation of the hybrids that we observe for A5–T15:A15 sample in Figure S8b.

Single-Stranded P15′:P15 Hybrids. To examine the trends in relative stabilities of single-stranded P15′:P15 hybrids in solution and when immobilized on gold, we compare responses of thiolated P15′–T5–P15–SH hairpins (Figure S9a) and end-tethered P15–T5–SH probes (Figure S9b) to several targets that can form complete or partial hybrids with both probes.

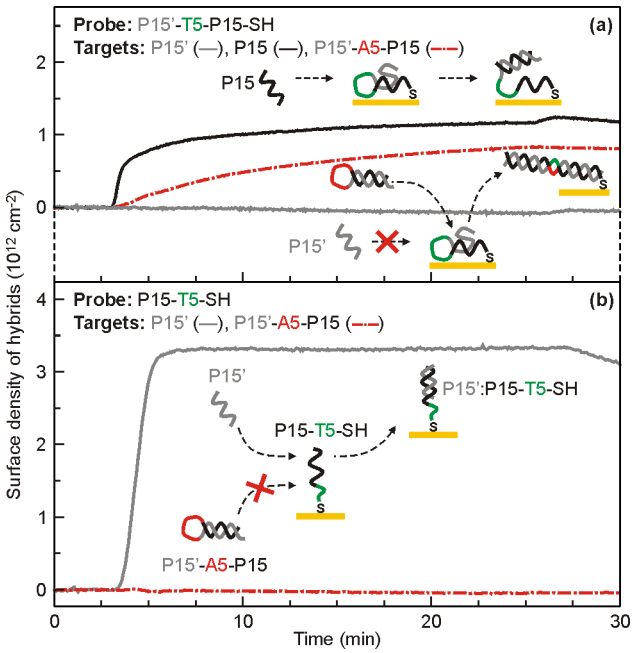

Figure S9. Asymmetric hybridization behavior of P15′–T5–P15–SH and P15–T5–SH probes exposed to full and partial complements in different conformations. SPR sensors functionalized with P15′–T5–P15–SH probes (a) were exposed to 4 μM solutions in NaCl-TE of three different targets: P15′ and P15 partial complements and P15′–A5–P15 full complement. For comparison, the simpler end-tethered P15–T5–SH probes (b) were exposed to P15′ and P15′–A5–P15 targets. Diagrams depict idealized representations of each target-probe pair (black = P15, gray = P15′, green = T15, red = A5) before and after hybridization. The line colors of the data plots correspond to the respective targets: black for P15, gray for P15′, and red dash-dot line for P15′–A5–P15.

We hypothesize that the thiol ligand on the P15 terminus of the P15′–T5–P15–SH hairpin forces the P15 block to interact with gold by proximity, making the P15–SH section analogous to the A15 "attachment block" in Figures 1c, S4–S6, and S8. Indeed, when exposed to the P15′ targets, the P15 blocks of the immobilized hairpins do not produce a detectable hybridization signal (gray line in Figure S9a). In contrast, the P15 targets can hybridize with P15′ blocks of the immobilized hairpins (black line in Figure S9a), albeit with a yield lower than that of A15–T20:A15 hybrids in Figure 1c.

The P15′:P15 hybrids enable us to expand the repertoire of probes and targets in competitive hybridization measurements: in addition to challenging hairpin probes with single-stranded targets (Figures 1, 3, S6), we also can challenge single-stranded probes (both folded and unfolded) with *hairpin targets* (red dash-dot lines in Figure S9). Figure S9b illustrates this approach for end-tethered single-stranded P15–T5–SH probes, which, of course, readily hybridize with P15′ targets (gray line in Figure S9b, cf. Figures S2 and S3). In contrast, P15′–A5–P15 *hairpin targets* that include the same P15′ target sequence do not produce any hybrids with the P15–T5–SH probes (red dash-dot line in Figure S9b), i.e., a hypothetical reaction that involves opening a solution single-stranded P15′:P15 hairpin hybrid to form an end-tethered *partial* double-stranded P15–A5–P15′: P15–T5–SH hybrid does not proceed. End-tethered *full* hybrids between P15′–A5–P15 targets and P15′–T5–P15–SH probes, however, are energetically favorable, as this type of hybridization proceeds in Figure S9a (red dash-dot line) despite requiring two hairpins to denature in the process.